Available online at www.sciencedirect.com
ScienceDirect
Microelectronic Engineering 84 (2007) 603–608
MICROELECTRONIC ENGINEERING
www.elsevier.com/locate/mee

Large-area submicron replica molding of porous low-*k* dielectric films and application to photonic crystal biosensor fabrication

Ian D. Block, Leo L. Chan, Brian T. Cunningham *

Nano Sensors Group, University of Illinois at Urbana-Champaign, 208 N. Wright St, Urbana, IL 61801, USA

Received 13 February 2006; received in revised form 14 December 2006; accepted 14 December 2006
Available online 16 January 2007

Abstract

We demonstrate a replica-molding method for submicron patterning of a low-index sol–gel nanoporous glass for the purpose of fabricating large-area (~80 cm^2) label-free photonic crystal optical biosensors. Scanning electron micrographs show the sol–gel exhibited minimal shrinkage and good substrate adhesion and depict precise and uniform pattern transfer over the fabricated area within the limits of measurement resolution. A unique characterization approach is described in which the photonic crystal optical resonance is used to accurately and quickly characterize the geometrical and material property uniformity over a large area. Uniformity within 1% was measured over an 80 cm^2 area. We suggest that this robust method is an excellent approach for photonic crystal sensor fabrication, and may also find applications in integrated optics and electronics.

Keywords: Low-*k*; Replica molding; Optical biosensor; Sol–gel glass

1. Introduction

Imprint lithography and nanoreplication methods are emerging as important techniques for imparting submicron features to a wide array of devices. In comparison to photolithography, and to a greater extent e-beam lithography, these methods provide higher throughput, lower cost, decreased processing complexity and equipment requirements, and the ability to directly pattern a large variety of materials [1]. This approach has previously been used to successfully mold sol–gel glass precursors into diffractive optical elements, lenses, and waveguides [2–4]. While porous low-*k* thin-films are important for interconnect dielectrics in IC manufacturing, their low refractive index also makes them attractive for optical device applications. In particular, we have found the low refractive index of porous dielectrics to be valuable for significantly increasing the sensitivity of a novel label-free photonic crystal optical biosensor [5]. Such photonic-crystal biosensors have previously been demonstrated for label-free detection of biochemical interactions, exhibiting a mass density sensitivity resolution of less than 1 pg/mm^2, refractive index discrimination down to 1×10^{-6} refractive index units (RIU), and a large dynamic range [6]. Detection of sub-nM analyte concentrations is required for drug discovery, environmental and food monitoring, and medical diagnostics, and at present challenges the quantitative limits of optical biosensors. Surface plasmon resonance (SPR) is currently the most widely accepted optical sensing technique and achieves refractive index resolution comparable to that of the device presented here, though the SPR platform is inherently limited in terms of throughput, cost, complexity, and portability [7].

In addition to the requirement of a low-index material, the biosensor application also mandates a sub-wavelength periodic surface structure, low-cost manufacturing for single-use disposable products, and a large surface area to enable incorporation within microplates and microarray slides. In this paper we present a nanoreplica molding pro-

* Corresponding author.
E-mail address: bcunning@uiuc.edu (B.T. Cunningham).

0167-9317/$ - see front matter © 2006 Elsevier B.V. All rights reserved.
doi:10.1016/j.mee.2006.12.011

cess for the purpose of fabricating enhanced sensitivity label-free optical biosensors, and show the successful scaling of these photonic crystal biosensors to a large-area microplate-based format. Using a unique characterization approach, we demonstrate the ability to uniformly pattern a sub-micron periodic surface structure into a low-index nanoporous sol–gel glass over a ~80 cm^2 area.

2. Fabrication

By adapting a sol–gel micro-molding process to a low-index porous glass precursor, we were able to design a low-cost, high-throughput process and avoid the use of photolithography. We chose to use polydimethylsiloxane (PDMS) as a molding tool because it has the beneficial properties of a low interfacial free energy, high flexibility and good chemical stability, enabling easy release from and accurate pattern transfer both from a rigid master mold and into the sol–gel material. Furthermore, the elastomeric material is gas permeable, allowing outgassing from the sol–gel upon curing without compromising pattern integrity [8]. Finally, the 275 nm feature size and ~0.6 aspect ratio we require lie safely under the resolution and aspect ratio limitations (100 nm and 2.0, respectively) of PDMS-based soft lithography [9,10].

An 8-in. diameter Si master wafer is patterned by deep-UV lithography with 96 circular grating regions (6-mm diameter) in an 8×12 rectangular grid at a pitch of 9 mm. This pattern layout of the silicon master wafer corresponds to the size and spacing of wells within a standard 96-well microplate. Each patterned area contains a linear grating with a 550-nm period, 170-nm depth, and 50% duty cycle etched into the Si by reactive ion etching. To facilitate release of the PDMS mold from the silicon wafer, the wafer is treated with a release layer of dimethyldichlorosilane. The wafer is first stripped of any organics in an oxygen plasma for 3 min at 300 W, then soaked in a solution of 2% dimethyldichlorosilane dissolved in octamethyl cyclooctasilane (Repel Silane, GE Healthcare) for 5 min, then finally rinsed with ethanol and deionized water. Sylgard 184 PDMS (Dow Corning) prepared in a 10:1 ratio is poured into an aluminum frame placed on the master, and then cured in a 90 °C oven for 24 h. After carefully separating the PDMS replica from the silicon mold, it is used to mold a thin film of uncured Nanoglass® (Honeywell Electronic Materials), a low-index sol–gel glass, spun-on to a 6-in.-diameter, 2-mm-thick borofloat glass wafer (Mark Optics) for 30 s at 2k RPM to produce a film thickness of 0.6 μm. The PDMS mold is carefully placed on the thin film and allowed to sit until the sol–gel visibly fills in the patterned PDMS. Once the low-index dielectric becomes rigid from a low-temperature cure (110 °C, 60 s), the flexible PDMS mold is removed and the sol–gel glass is fully cured by further baking (350 °C, 5 min). The PDMS mold can be used tens of times before significant grating line collapse or defect and particulate accumulation are observed. The sensor structure is completed by evaporating 165 nm of TiO_2 onto the patterned surface. An automated precision dispensing machine (EFD) is used to apply a UV curable epoxy onto a bottomless 96-well standard microtiter plate (Greiner) for bonding to the sensor once the circular glass wafer has been cut to the appropriate rectangular size (11.0×7.5 cm^2). A process flow diagram illustrating the fabrication process is given in Fig. 1a–e.

After TiO_2 deposition, the completed device behaves as a polarization-dependent narrowband reflectance filter. Upon illumination at normal incidence with collimated white light, only a single resonant wavelength is reflected with ~100% efficiency, while all other wavelengths are transmitted through the structure [11]. An illustration of the device cross-section geometry and operation principle are given in Fig. 2a and b, respectively. The reflected intensity at wavelengths other than the resonant wavelength is due to reflection from the back surface of the device substrate, which is not treated with an antireflection coating. The spectral location of peak reflection, or peak-wavelength-value (PWV), is readily tuned by changes in the optical density of the medium above the sensor surface lying within the range of the evanescent electric field. Therefore, bulk refractive index (RI) changes of the cover medium will induce a shift in the PWV, as will any thickness or density changes of a surface-bound biomolecular layer. Furthermore, the spectral location of this peak wavelength value (PWV) is heavily dependent upon device geometry and material properties, including the grating refractive index, depth, duty cycle, and period [12,13]. Since

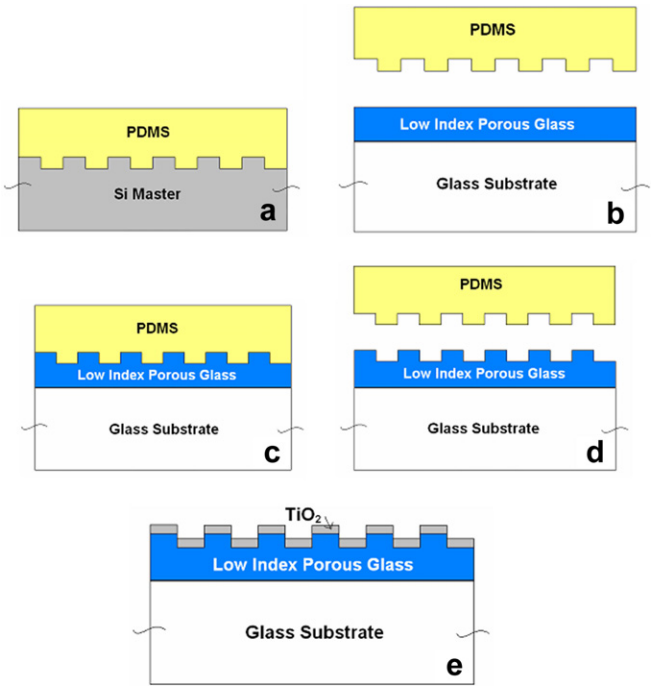

Fig. 1. Porous glass photonic crystal sensor process flow. (a) Cast mold polydimethylsiloxane (PDMS) from silicon master patterned by DUV lithography, (b) spin-on 600 nm low-index sol–gel glass onto glass wafer, (c) mold sol–gel using PDMS and heat-cure, (d) remove mold, perform additional curing, and (e) complete device by depositing TiO_2.

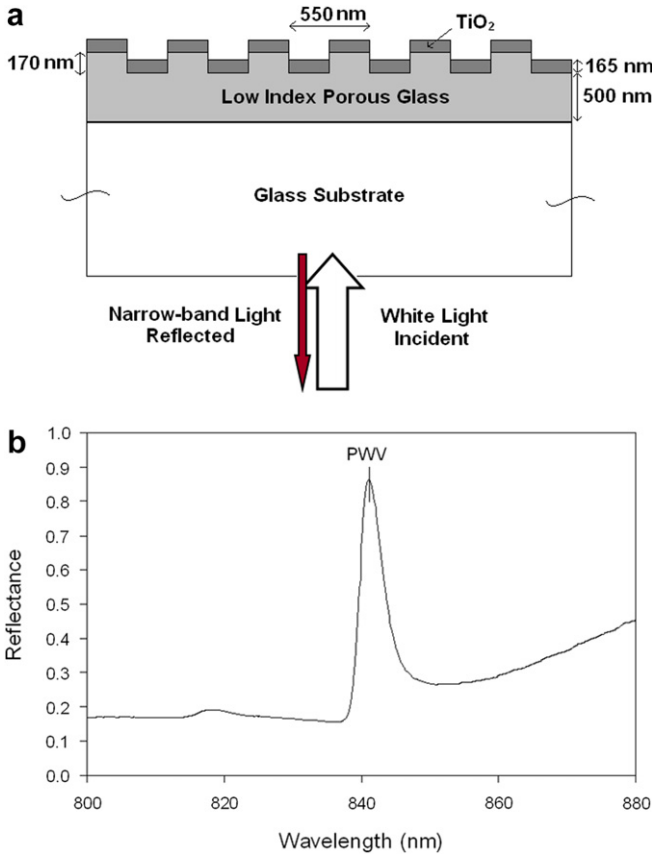

Fig. 2. (a) Cross-section schematic of porous-glass photonic crystal optical biosensor, and (b) measured reflectance spectrum for the device immersed in water.

the optical changes induced by biomolecular adsorption are small, minimizing structural and material variations across the entire sensor surface is crucial to ensuring uniform and robust biosensor operation.

3. Results and discussion

Scanning electron microscope (SEM) images of molded porous glass grating structures with a period of 550 nm are shown in Fig. 3a and b. The sol–gel exhibited minimal shrinkage and good substrate adhesion during curing and mold removal stages. SEM images reveal uniform and accurately patterned structures over the inspected areas within the limits of measurement resolution. While spot SEM measurements can provide information on local replication quality, the long-range uniformity over the immense nanostructured area cannot be inspected with traditional characterization tools. However, because the PWV and the sensor sensitivity are strongly dependent upon the geometry and material properties of the device, they provide an extremely sensitive and efficient method by which to investigate replication quality and uniformity over a large area.

The porous glass photonic crystal sensor was further characterized using an imaging instrument that produces a spatial PWV map of the sensor surface with an $89.2 \times 89.2\ \mu m^2$ pixel resolution. Because the sensor structure strongly confines light at the resonant wavelength, high spatial resolution can be achieved. A detailed description of the imaging instrument used in this work has been given previously [14].

The sensor shown in Fig. 4a was bonded to a bottomless 96-well standard microplate for compatibility with the characterization instrumentation. Using the imaging system to produce the spatial PWV map in Fig. 4b, we find that the average PWV across each 6 mm well of the microplate-bonded sensor filled with deionized water is 870.38 ± 2.73 nm, and the average standard deviation across each well is ± 0.31 nm.

In order to relate measured PWV variations to physical sensor parameters, we ran rigorous coupled wave analysis (RCWA) simulations to determine the change in PWV due to perturbations of the grating dimensions. RCWA computer simulations have proven to be an accurate tool for modeling photonic crystal biosensor resonant reflection wavelength, peak width, and sensitivity provided that the model parameters match the measured structure [5]. The results are summarized in Table 1. The PWV standard deviation measured across the entire $\sim 80\ cm^2$ area of the actual device was only $\pm 0.31\%$. While we can extract the holistic replication uniformity across a large area very quickly by using a PWV imaging instrument, we cannot directly determine the precise contribution of each potentially variable geometrical or material property to the non-uniformity. However, ellipsometric measurements of molded nanoporous glass samples show refractive index uniformity within $\pm 0.07\%$. Furthermore, spot SEM measurements indicate no measurable grating period, duty cycle, or grating height variations. The TiO_2 coating exhibited a thickness and refractive index gradient across the face of a 6″ substrate with standard deviations of $\pm 1.0\%$ and $\pm 0.7\%$, respectively. Based on the aforementioned data and the simulation predictions given in Table 1, we speculate that the source of PWV non-uniformity arises from two distinct sources. The global variations in PWV across the wells of the microplate-based sensor result from non-uniformity of the evaporated TiO_2 film. PWV variability within single wells are more likely a result of defects and minute grating period variations due to local stresses placed on the PDMS tool during pressure application. Defects and contaminants on the daughter mold would give rise to sensor defects while particulates between the PDMS and pressure applicator may cause local variations of the grating periodicity.

While the absolute PWV measurements give an indication of physical sensor properties, the device response to a bulk index change provides a measure of biosensor sensitivity. Increased refractive index of the liquid in contact with the sensor surface induces a positive shift of the PWV. By subtracting subsequent scans of the microplate-based sensor containing wells filled with deionized water ($n = 1.333$) and then with isopropyl alcohol ($n = 1.378$),

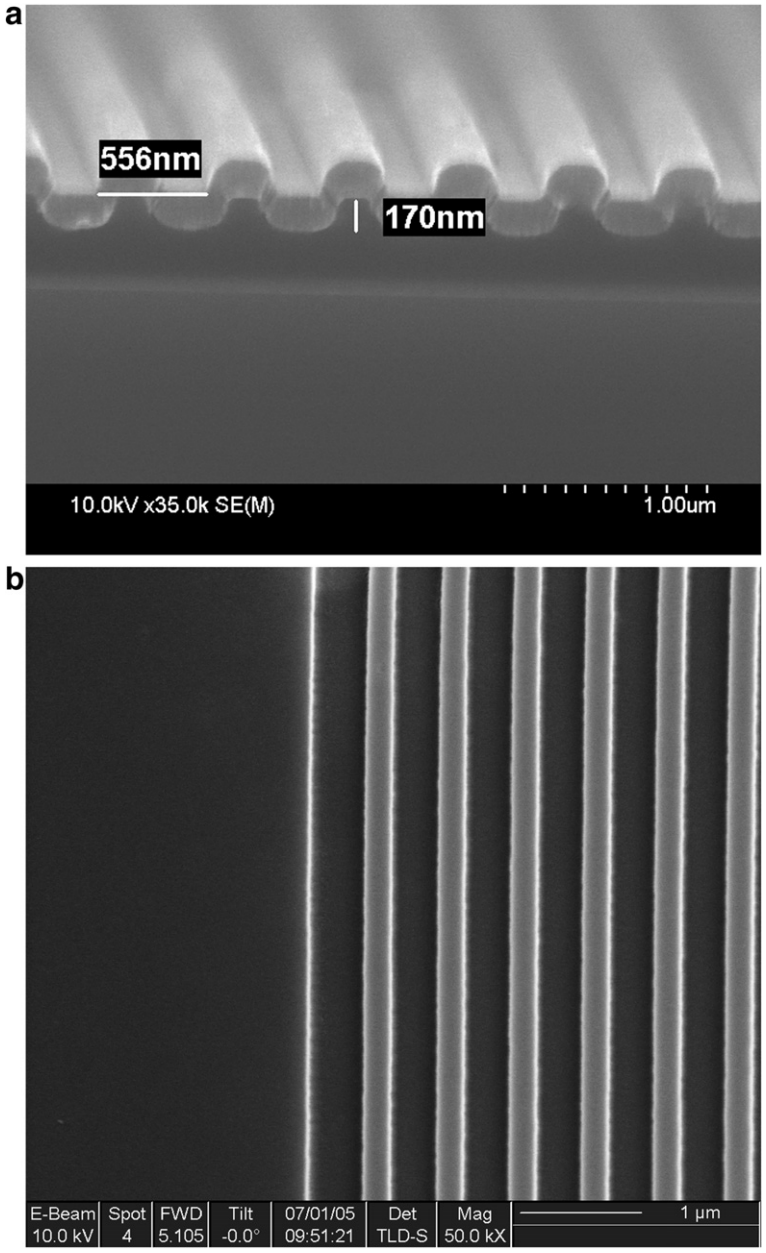

Fig. 3. Scanning electron micrograph (SEM) of photonic crystal optical biosensor cross-section (a) and top-view (b).

we can map the bulk index-induced PWV shift across the whole sensor area. Though this type of bulk index test is common for characterizing optical biosensors, it does not provide a complete description of how the sensor will interact with the test volume.

Typical affinity assays with surface-immobilized ligands rely on biochemical binding that occurs within several hundred nanometers of the sensor surface. We therefore sought to characterize the near-surface sensitivity uniformity of the sensor by depositing a self-limiting monolayer of Poly(Lys, Phe) (PPL; Sigma–Aldrich; MW = 35,400 Da) prepared to a 0.5 mg/ml solution with 0.01 M phosphate buffered saline (PBS; pH 7.4) in each well of the microplate-based sensor [15]. After establishing a baseline PWV with only PBS in the test wells, the buffer was replaced with PPL solution and was allowed to stabilize for 30 min. The PPL solution was subsequently removed, the wells were rinsed to eliminate weakly bound molecules and finally refilled with fresh PBS. The resulting PWV shift induced by PPL monolayer adsorption is reported alongside the bulk shift data in Fig. 5. These surface and bulk sensitivity data agree well with results obtained from the previous characterization of microscope slide-based porous-glass photonic crystal biosensors. The successful scaling of the fabrication process presented here to a microplate-based format will enable the use of this biosensor in low-cost, high-throughput biomolecular screening assays.

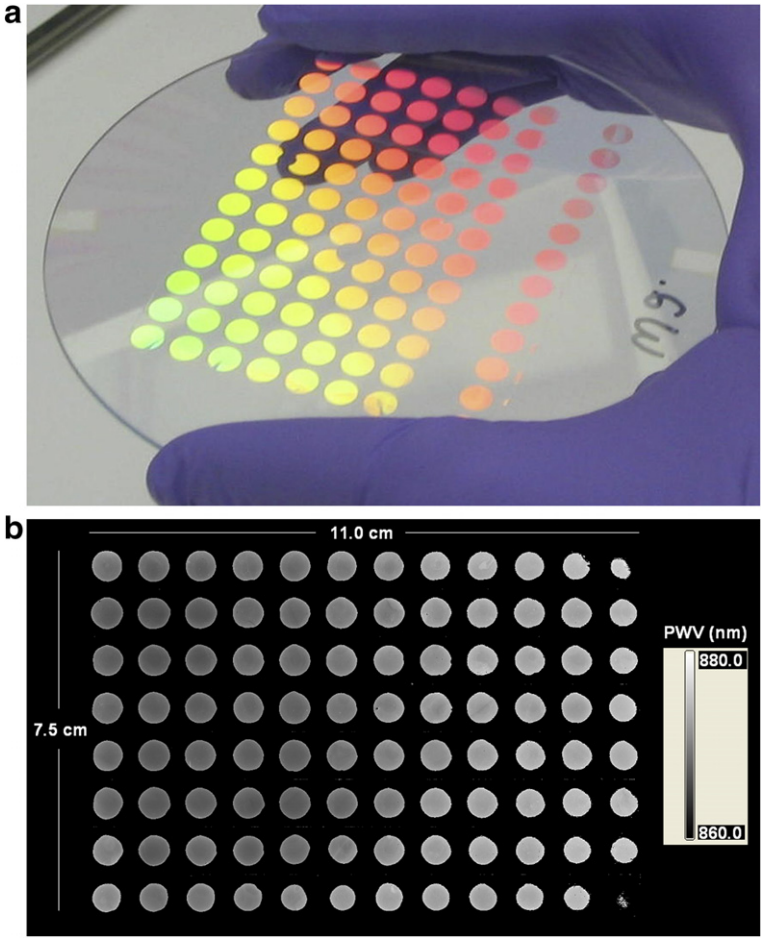

Fig. 4. (a) 96-Well label-free biosensor format. (b) Spatial PWV image map of photonic crystal sensor bonded to microplate filled with deionized H_2O. Dark regions signify locations where no reflected resonance is obtained.

Table 1
Change in PWV due to a 1% perturbation in geometrical and material properties of the photonic crystal biosensor, as predicted by RCWA simulation

1% Parameter variation	Simulated ΔPWV (nm)
Duty cycle	0.1
Height	0.4
Period	7.3
Porous glass RI	1.9
TiO_2 RI	1.3
TiO_2 thickness	1.5

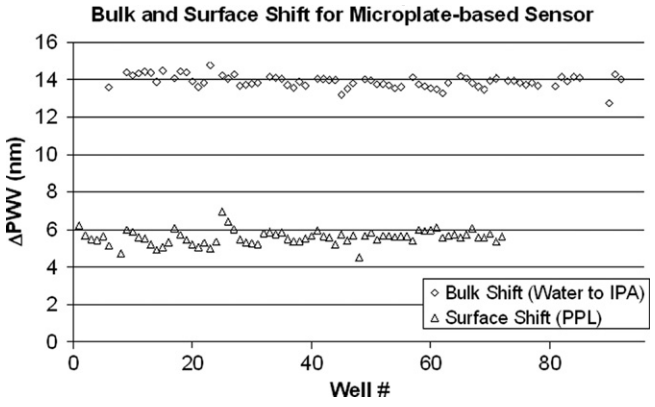

Fig. 5. PWV shift endpoint plot for bulk solution exchange between deionized H_20 and isopropyl alcohol (IPA) and for PPL monolayer adsorption. Wells shown without data were used for reference.

Although we have demonstrated the successful application of a large-area nanoporous glass patterning approach to a photonic crystal biosensor, other fields may also benefit from this technique. The method presented in this paper will enable the low-cost high-resolution patterning of low-k sol–gels for inclusion in nano- and micro-optical components. Furthermore, the integrated circuit industry may see benefits in pursuing micro-molding as a low-cost alternative for low-k dielectric patterning.

While there is significant latitude in the application of this technique to structures other than that presented here, it is not unlimited. The high coefficient of thermal expansion and low Young's modulus of PDMS may pose problems for alignment of multilayer structures and will inherently limit the achievable resolution and aspect ratio [16].

4. Conclusions

We have successfully developed a low-pressure, low-temperature elastomeric nanoreplica molding process for the purpose of fabricating a large-area 550 nm periodic low-index nanoporous sol–gel glass structure. We have characterized the structure as implemented in a photonic crystal biosensor, providing a very precise measure of pattern accuracy and uniformity. This fabrication method shows great promise for the described device as well as the extension to other applications in integrated optics and electronics.

Acknowledgements

The authors gratefully acknowledge the National Science Foundation (BES 04-27657) and SRU Biosystems for providing financial support for this work, and Honeywell Electronic Materials for the donation of Nanoglass® low-*k* porous dielectric material. FIB work was carried out in the Center for Microanalysis of Materials, and thin-film characterization was performed in the Laser and Spectroscopy Facility of the Frederick Seitz Materials Research Laboratory, both at the University of Illinois and both of which are partially supported by the US Department of Energy under grant DEFG02-91-ER45439. The authors also extend their gratitude to the support staff of the Micro and Nanotechnology Laboratory at the University of Illinois at Urbana-Chamapaign.

References

[1] M. Geissler, Y. Xia, Advanced Materials 16 (2004) 1249–1269.
[2] C. Marzolin, S.P. Smith, M. Prentiss, G.M. Whitesides, Advanced Materials 10 (1998) 571–574.
[3] S. Obi, M.T. Gale, A. Kuoni, N.D. Rooij, Microelectronic Engineering 73–74 (2004) 157–160.
[4] V.K. Parashar, A. Sayah, M. Pfeffer, F. Schoch, J. Gobrecht, M.A.M. Gijs, Microelectronic Engineering 67–68 (2003) 710–719.
[5] I.D. Block, L.L. Chan, B.T. Cunningham, Sensors and Actuators B 120 (2006) 187–193.
[6] B. Lin, P. Li, B.T. Cunningham, Sensors and Actuators B 114 (2006) 559–564.
[7] R. Karlsson, R. Stahlberg, Analytical Biochemistry 228 (1995) 274–280.
[8] Y. Xia, G.M. Whitesides, Annual Review of Materials Science 28 (1998) 153–184.
[9] E. Delamarche, H. Schmid, B. Michel, H. Biebuyck, Advanced Materials 9 (1997) 741–746.
[10] M. Bender, U. Plachetka, J. Ran, A. Fuchs, B. Vratzov, H. Kurz, T. Glinsner, F. Lindner, Journal of Vacuum Science and Technology B 22 (2004) 3229–3232.
[11] R. Magnusson, S.S. Wang, Applied Physics Letters 61 (1992) 1022–1024.
[12] B.T. Cunningham, P. Li, B. Lin, J. Pepper, Sensors and Actuators B 81 (2002) 316–328.
[13] B.T. Cunningham, J. Qiu, P. Li, J. Pepper, B. Hugh, Sensors and Actuators B 85 (2002) 219–226.
[14] P. Li, B. Lin, J. Gerstenmaier, B.T. Cunningham, Sensors and Actuators B 99 (2004) 6–13.
[15] C. Picart, G. Ladam, B. Senger, J.-C. Voegel, P. Schaaf, F.J.G. Cuisinier, C. Gergely, Journal of Chemical Physics 115 (2001) 1086–1094.
[16] M. Tormen, T. Borzenko, B. Steffen, G. Schmidt, L.W. Molenkamp, Microelectronic Engineering 61–62 (2002) 469–473.